ARTICLE

Check for updates

Multi-port real-time observation for ultrafast intracavitary evolution dynamics

Yufan Du[1,2,3], Liao Chen[1,2,3], Zihui Lei[1,2], Chi Zhang [1,2✉], Luming Zhao [1✉] & Xinliang Zhang [1,2✉]

Recent advances in real-time spectral measurements of a mode-locked fiber laser have found many intriguing phenomena and which have verified the soliton theory. However, most current results are based on laser single-port observation, and are rarely involved in the cavity evolution, which also has rich nonlinear dynamics according to the soliton theory. Here we present an approach for the intracavity soliton evolution processes, where spectra from multi-ports are collected in time-division multiplexed sequence to realize synchronous real-time observation. The sinusoidal evolution of the spectral beating is observed clearly, agreeing with the reported prediction. Furthermore, the intracavity spectral dynamics of the period-doubling bifurcation are also revealed. Our scheme observed the spectral expanding and shrinking alternately and periodically over two round trips, matching well with simulations. This work may open up possibilities for real-time observation of various intracavity nonlinear dynamics in photonic systems.

[1] Wuhan National Laboratory for Optoelectronics & School of Optical and Electronic Information, Huazhong University of Science and Technology, Wuhan 430074, China. [2] Optics Valley Laboratory, Wuhan 430074, China. [3] These authors contributed equally: Yufan Du, Liao Chen. ✉email: chizheung@hust.edu.cn; lmzhao@ieee.org; xlzhang@mail.hust.edu.cn

Solitons in mode-locked fiber lasers, the result of combined factors such as gain, loss, dispersion, and nonlinearity, are under intense research focus[1–4]. Complex dynamics of solitons will be shown when these factors are not yet or out of balance. Many interesting soliton dynamics phenomena have been predicted theoretically and successfully implemented in simulations, such as soliton explosions[5] and pulsating solitons[6]. Recently, real-time spectral measurement technology, such as the time-stretched dispersion Fourier transform (TS-DFT), maps the optical spectra of solitons into temporal waveforms, which makes the observation of the ultrafast soliton dynamics possible[7–16]. With the help of the TS-DFT, phenomena such as soliton molecular[17,18], breathing soliton dynamics[19], soliton rain[20,21], and rogue waves[22] have been successfully observed in real-time.

It is worth noting that most of the current experimental work can be attributed to the observation of soliton dynamics outside the cavity, for the solitons undergo a whole round trip. In fact, there are various fibers and devices distributed in the cavity, and the solitons must be affected differently when they pass through each part, thus showing distinct characteristics[23,24]. Therefore, the current single-port spectra measurements are likely to be unable to observe the fast-changing intracavity processes in detail and even miss some phenomena with short-lived evolution processes. It is easy to extract the spectra of any point in the cavity from numerical simulation; however, increasing observation points in experiments is often achieved by adding an optical coupler (OC) and the additional measurement links will introduce the influence of the measurement devices, such as the amplification process in the erbium-doped fiber amplifier (EDFA). Moreover, for the fast-changing and short-lived mode-locking state, how to obtain the absolute values of the wavelength to observe the spectral evolution of the soliton more accurately is also a difficult problem[25]. Thus, although many numerical simulations have shown that the property of solitons at different positions in the cavity is significantly different[26–29], there are few experimental researches on the dynamics of intracavitary solitons. The real-time observation of intracavitary soliton dynamics is essential to observe a more complete soliton evolution process, which is necessary to better understand the transient characteristics of solitons.

In this work, we increase observation ports and introduce a fiber Bragg grating (FBG) as the trigger of multi-signal to realize multi-port synchronous real-time observations, which improves the sampling rate and reveals the intracavitary process more clearly. Experiments show that the solitons output from different ports have similar build-up processes as a whole, while the spectra of different ports have obvious differences at the same round trip. In the modulation instability stage, many sub-pulses coexisting with the main pulse have different numbers, intensities, and positions at different output ports. In the spectral beating phase, the solitons output from different ports are in different beating states and the beating process shows a continuous sinusoidal evolution after rearranging the spectra in sequence. Besides, the dynamics of Kelly sidebands and peaks induced by self-phase modulation (SPM) are also reflected by multi-port observation, which is asynchronous with the soliton. The simulation of the complete intracavitary evolution process shows that their evolution processes are also approximately sinusoidal, and the periods are shorter than that of the soliton beating process, which means that a higher sampling rate is required to experimentally observe their evolution details. Subsequently, the spectral coherence of solitons output from different ports in a steady state is characterized, and as expected their spectral coherence also evolves periodically in the cavity. Finally, the intracavitary spectral dynamics of the period-doubling bifurcation are demonstrated. The spectrum is periodically compressed and broadened in two round trips, and the outputs from different ports describe how soliton evolves in the cavity. Numerical simulations agree with the experiments and indicate that the characteristic spectra captured by the multi-port can be used to describe the more realistic evolution process in the cavity.

Results

Principle. The principle of multi-port real-time observation is shown in Fig. 1a. Under the action of the intracavity gain and the saturable absorption effect caused by the nonlinear device, the dominant pulse, that is the soliton gradually forms. At this time, the real-time spectra of the pulse can be discretely observed by the DFT technique. However, the evolution of the pulse in the cavity is a continuous process (Fig. 1b), and the single-port observation can only reflect the spectra of the pulse when it passes through a fixed point in the cavity, so the spectral information of the intermediate process is lost due to the insufficient sampling rate (Fig. 1c). The multi-port observation can shorten the interval of observation windows, thereby increasing the sampling rate and characterizing a more complete spectral evolution process. Further, if the relative position of the observation point in the cavity is also considered, it can reflect a more real spectral evolution process (Fig. 1d).
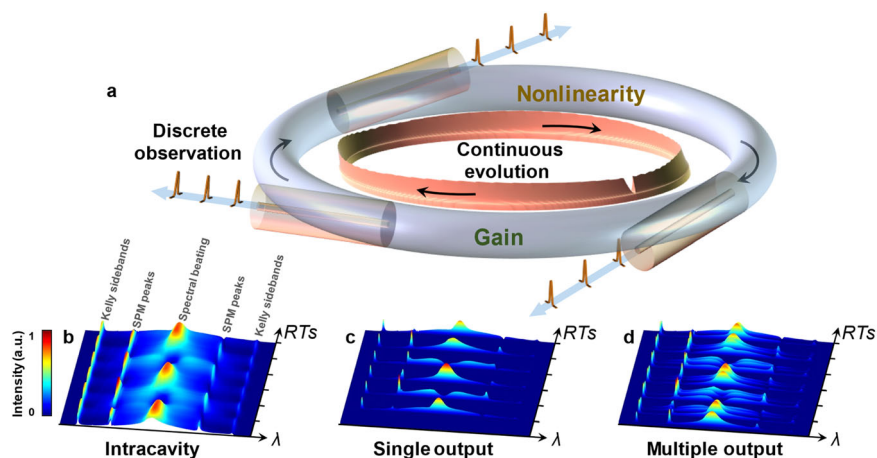

Fig. 1 Principle of multi-port real-time observation. a Soliton evolves continuously in the cavity and (**b**) the spectral beating process of intracavity soliton from simulation (the detailed simulation parameters are shown in Table 1). RT: round trip. **c** Discrete observation by single output reflects an incomplete spectral beating process and (**d**) Multiple output observation increases the sampling rate to show details of the soliton evolution process.
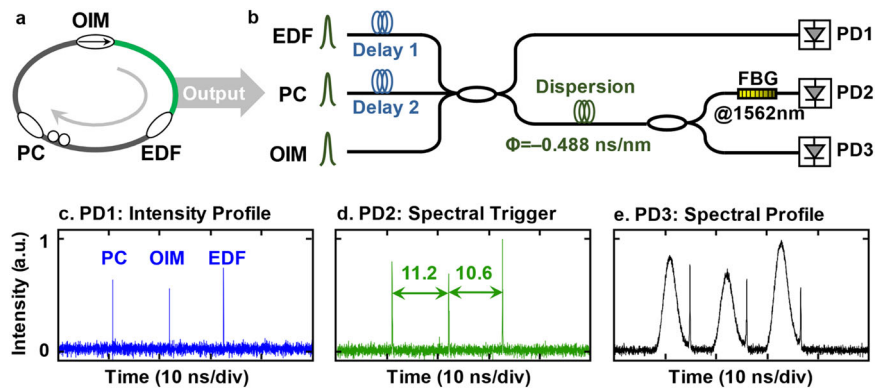
Fig. 2 Experimental setup of multi-port real-time observation. a The laser setup and (**b**) The detection system. Spectra from multi-ports are collected in time division multiplexed sequence. OIM optical integrated module, EDF erbium-doped fiber, PC polarization controller. PD photodetector, FBG fiber Bragg grating. **c** The multiplexed pulses train is well-resolved. **d** The narrow pulses generated by the FBG are used as the spectral triggers. **e** The stretched spectra.

Table 1 The parameters used in the numerical simulation of the spectral beating process.

	SMF	EDF	HI1060
$\theta = 110/180\pi$	$\beta_2 = -21.7$ ps^2 km^{-1}	$\beta_2 = 64$ ps^2 km^{-1}	$\beta_2 = -11.4$ ps^2 km^{-1}
$\varphi = 282/360\pi$	$\beta_3 = 0.1302$ ps^3 km^{-1}	$\gamma = 0.0066$ W^{-1}	$\beta_3 = 0.1302$ ps^3 km^{-1}
$L_b = 1$ m	$\gamma = 0.00146$ W^{-1}	Gaussian shape	$\gamma = 0.00165$ W^{-1}
$\lambda_0 = 1560$ nm	$L = 9.75$ m	FWHM $= 30$ nm	$L = 0.5$ m
		$g_0 = 20$ m^{-1}	
		$L = 0.45$ m	
		$E_s = 51.9$ pJ	

SMF single-mode fiber, *EDF* erbium-doped fiber.
HI1060: Corning HI1060 fiber. φ is the additional phase shift introduced by the polarization controller (PC), and θ is the angle between the polarization direction of the optical integrated module (OIM) and the slow axis of the fiber. L_b is the average linear birefringence beat length of the fiber laser resonator, and $\lambda 0$ is the center wavelength. $\beta 2$ is the dispersion of the fiber and $\beta 3$ is the third-order dispersion. γ is the nonlinear coefficient of the fiber. g_0 is the small-signal gain and E_s is the gain saturation energy related to pump power. L is the fiber length.

As a test-bed system, a typical dissipative soliton fiber laser with three output ports is built (Fig. 2a). A 0.45-m long segment of erbium-doped fiber (EDF) is used as the gain medium. A 0.5-m long HI1060 fiber is used as the pigtail of the polarization-dependent optical integrated module (OIM) to connect with the EDF. To reduce the effect of coupling loss on the soliton evolution processes, the coupling ratio of the coupler is chosen as 90:10. In this case, the introduction of couplers indeed introduces the loss but will not have much effect on the evolution trend, which is verified by the simulation in advance. In addition, the nonlinear effect introduced by the coupler can be ignored, for the length of the coupler is much smaller than the total cavity length. The two 90:10 OCs are employed after EDF and the polarization controller (PC) respectively to tap 10% of the laser power out of the cavity. The rest of the laser cavity is single-mode fiber (SMF) and the total cavity length is 10.7 m. An analog modulated 980-nm pump laser module is used as a pump source.

To solve the aforementioned problems, the detection link is optimized, see Fig. 2b. Considering that the cavity length of the laser is 10.7 m, corresponding to a cavity round-trip time of about 50 ns, coupling the three outputs into one and adjusting the delay for optical time-division multiplexing[30,31] allows three signals to pass through the same measurement link to eliminate the influence of additional links. The multiplexed pulse train is well-resolved with fairly stable inter-pulse separation (Fig. 2c). Since the three pulses are output from different positions in the cavity, the pulse from the EDF port belongs to the next round trip. But in the experiment, for the sake of convenience, three

adjacent pulses are demultiplexed as a group and then rearranged. Dispersion compensating fiber (DCF) is used to stretch the multiplexed pulse (EDFA is undrawn) and the stretched pulses are split into two parts by OC (80:20), where one port is detected with a high-speed 40 GHz photodiode (PD) plugged into a 59-GHz 160-GSa/s real-time oscilloscope (DSAZ594, Keysight) to observe the real-time spectra (Fig. 2e). The other port enters the oscilloscope after passing through FBG with a bandwidth of 0.25 nm, thereby obtaining a narrow pulse as an accurate wavelength trigger (Fig. 2d), allowing the spectra of the three ports to be synchronized in the time domain, which makes it easier to identify their differences. The minimum interval between adjacent spectra is 10.6 ns, in other words, an observation bandwidth of 20.5 nm can be achieved with a total dispersion of $\Phi = -0.488$ ns/nm.

Soliton formation dynamics. After adjusting the PC to achieve stable mode-locking, a 50-Hz square wave electrical signal is used to control the self-starting process of the laser. Here, one of the soliton formation dynamics is demonstrated in Fig. 3a. The experimental results show that there is a long-time relaxation oscillation (RO)[32,33], and then after the Q-switched mode-locking, a stable mode-locking is gradually formed. Take the output of the OIM port as an example, the illustration shows a good fit between the single-shot spectra during stable mode-locking captured by the DFT method (red solid line) and the average spectra captured by the optical spectrum analyzer (OSA, blue solid line). The different intensity of the Kelly sideband is mainly because of the limited resolution of the DFT method. Dissipative soliton formation dynamics mainly exist between the Q-switching mode-locking and stable mode-locking stage[34]. Therefore, the demultiplexed outputs of this process (around 7000 round trips (RTs)) are displayed separately in Fig. 3b. Five different physical processes involved in the build-up phase can be seen. During the initial stage of the evolution (up to RT number 1020), the strongest main pulse coexists with many small pulses of varying intensities. On the next stage of the evolution (stage 2, RTs ~1020–1400), the strongest main pulse quickly expands into a wide-bandwidth signal, the dissipative soliton is initially formed, and the small pulses gradually disappear. However, the soliton at this time is not stable. Spectral beating caused by SPM[29] forms three sidebands (RT number 1600) and causes the soliton splitting into a small pulse (stage 3, RTs ~1800–2100), which shows up as interference fringes on the spectra. After a long beating (stage 4, RTs ~1600–6500), the soliton finally stabilizes, forming a stable mode-locking (stage 5). Take the output of the OIM port as
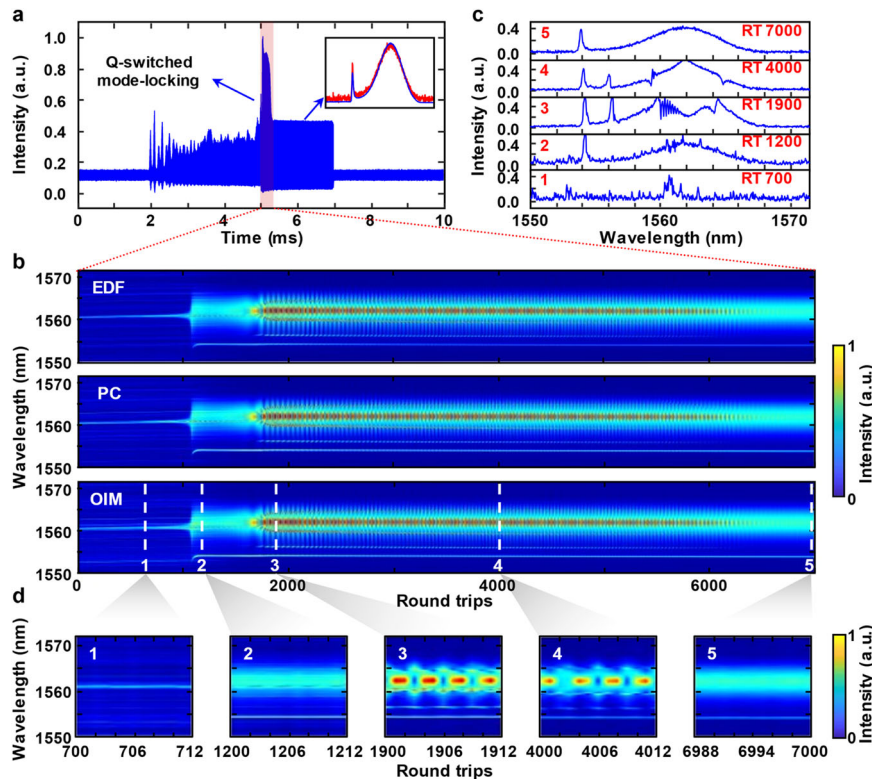
Fig. 3 Soliton formation process. a Spectral information captured by the DFT method. **b** The real-time evolution process of the soliton establishment, including 5 different physical processes. The output of the three ports is different in detail. EDF erbium-doped fiber, PC polarization controller, OIM optical integrated module. **c** Typical cross-sections of the spectra. The drift of the Kelly sideband can be observed owing to the accurate spectral trigger. **d** Zoom in spectral evolution of 5 stages.

an example, Fig. 3c displays the typical cross-sections of the spectra at RT numbers of 700, 1200, 1900, 4000, and 7000 and the zoom in the real-time evolution process of 5 stages in Fig. 3d can better reflect the evolution characteristics of these processes. Note that since the absolute value of the wavelength has been obtained, the drift of the Kelly sideband can also be observed during these evolutions, and the total drift is about 0.3 nm.

The difference of soliton in different cavity position is also shown by multiple outputs. As mentioned earlier, the strongest main pulse coexists with many sub-pulses of varying intensities resulting from modulation instability introduced by random noise in the initial stage[29]. Due to the large pulse width (~tens of ps), DFT cannot map the spectra of sub-pulses to the time domain, therefore their time-domain information is preserved in the stretched spectra[35]. In this experiment, the numbers and positions of the sub-pulses of three ports are different (Fig. 4a–c), while the positions and intensity of the sub-pulses at the same port evolve slowly, which indicates these sub-pulses have a cyclical evolution in the cavity. A large number of experimental results also show that the positions and numbers of the sub-pulses of three ports are random during each establishment of the soliton. Although the spectral information of these sub-pulses cannot be obtained by DFT in this experiment, their character-istic of evolving asynchronous with the soliton and recurring in the cavity can be further studied by other methods, for example, in combination with time lens techniques.

In the spectral beating stage, 12 consecutive spectra of the three ports are shown to reveal their differences (RTs ~4004–4015). The outputs of different ports show a clear but uneven beating process and at the same round trip, they are at different beating states (Fig. 4d–f), which verifies that the spectral beating process of the soliton is a continuously evolving process. Therefore,

considering the relative position of each port in the cavity, after arranging the three output signals in sequence, reconstituted spectra show a more regular spectral beating process (Fig. 4g), which is quite consistent with the simulation results in the schematic. The multi-port observation can clearly show that the soliton beats 4 times in these 12 RTs, which cannot be accurately judged by the single-port observation. Owing to the improvement of the sampling rate, the beating process of the Kelly sidebands and the shifting process of the SPM peaks are also reflected, which are also asynchronous with the soliton. Although the simulation of the complete intracavity evolution processes in Fig. 1b has shown that their evolution processes are also approximately sinusoidal, their experimental observation requires a shorter interval of observation windows due to their faster evolution period compared with the spectral beating process of the soliton. It is worth noting that the SPM peaks gradually drift away from the center wavelength as a whole (Fig. 3b), but in each beating, they always drift toward the center wavelength first, and then the next peaks are slightly further away from the center wavelength. Moreover, taking the intensity at the central wavelength position (1562 nm) to represent the intensity change of the beating process, it can be found that the beating process exhibits an approximately sinusoidal period of about 3.33 round trips (Fig. 4h). The green, blue, and orange dots represent the outputs of the EDF, PC, and OIM ports, respectively. Just looking at the dots of one color, it is difficult to get such a complete sine curve. It should be noted that the spectral beating process of the soliton from the simulation in Fig. 1d is also sinusoidal, but its period is about 2.4 round trips. This is mainly because that the nonlinear accumulation process is extremely dependent on the initial conditions, and it is difficult to find the initial conditions that exactly match the experiment in the simulation. However, no
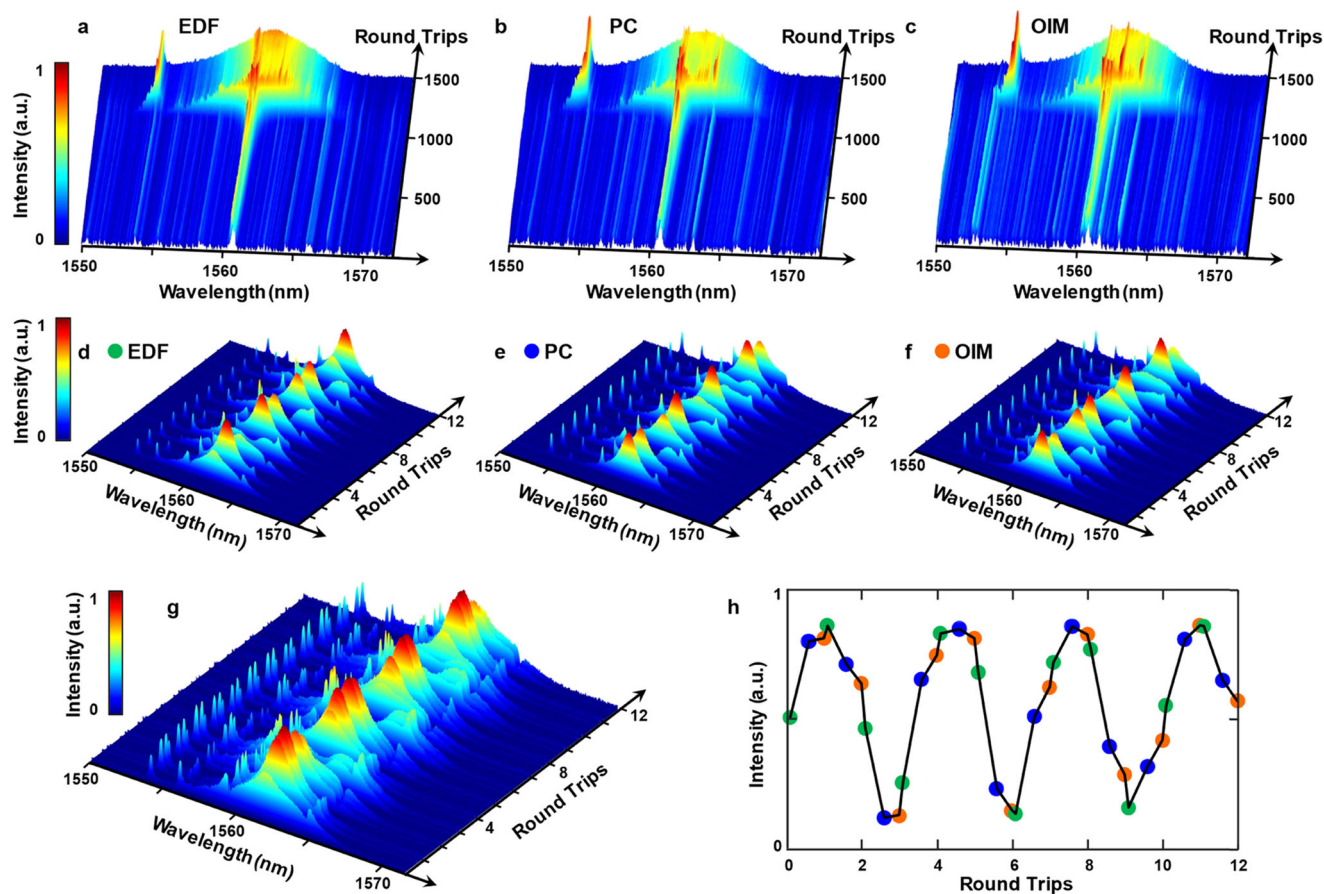
Fig. 4 The soliton dynamics of different ports. a–c are the output of the EDF, PC, and OIM ports in the initial stage respectively. Sub-pulses have a cyclical evolution in the cavity, which is asynchronous with the soliton. EDF erbium-doped fiber, PC polarization controller, OIM optical integrated module. **d–f** are 12 consecutive spectra in the spectral beating phase for the EDF port, PC port, and OIM port respectively. The spectral beating process is obvious but irregular and soliton in different ports are at different beating states. **g** The reconstituted spectra show a regular beating process and many other details. **h** The intensity evolution process at the central wavelength position, is approximately a sinusoidal evolution process with a period of about 3.33 RTs. The green, blue, and orange dots represent the outputs of the EDF, PC, and OIM ports, respectively.

matter what the initial conditions are, the nonlinear devices in the cavity will exert different modulation effects on the soliton. The beating of the soliton makes it continuously approach the equilibrium state of these interactions, and finally reach a steady state.

Spectral coherence of solitons. In addition to the dynamic differences, there are also differences in the steady-state properties of intracavity soliton. The spectral coherence of soliton of different ports, that is, the stability of the intensity and phase between adjacent femtosecond pulses, is measured by time-domain stretching interferometry method[36,37]. 500 consecutive interferometric stretched pulses are stacked in the same window as Fig. 5a–c shown. The entire observation window is about 0.026 ms, so it is normal for the pulse to have slight intensity disturbances on such a time scale. Therefore, their average value (the black solid line) is called the one-dimensional interferogram. Due to the difference of the pulse energy, the overall intensity of the interferogram of the three ports has a certain difference. Near the central wavelength, the interference fringe depths of the EDF, PC, and OIM output ports increase sequentially, indicating that their one-dimensional spectral coherence increases sequentially.

The two-dimensional (2D) interferogram can be calculated from the one-dimensional interferogram, which reflects the coherence between any two wavelength components (Fig. 5d–f). 2D interferograms for all three ports show a well-defined square-

grid pattern with high contrast for the high visibility of the interference fringes across the spectra. In order to show the difference between the three ports more clearly, the estimated cross-spectral density (CSD) functions are recovered from the visibilities of 2D spectral interferograms in Fig. 5g–i[37]. The closer the color is to red, the closer the CSD is to 1. As expected, the regions around the central wavelength of the three ports all show a high degree of coherence correlation, which is manifested as the large square area with CSD close to 1.0. Two striped regions that also show high coherence, which is Kelly sidebands. But relatively speaking, the color of the EDF port is lighter, and the square area as well as the striped area are smaller than that of the other two ports, indicating that the 2D coherence of the EDF port is relatively poor.

These differences indicate that the spectral coherence of soliton also has an evolutionary process in the cavity. The gain medium provides gain while the spectral coherence is degraded, and subsequently, the spectral coherence is continuously enhanced due to the saturable absorption caused by PC and OIM. Such spectral dynamics potentially induced by intracavity nonlinear devices deserve to be of interest, especially as the structure of the laser becomes more complex.

Period-doubling bifurcation. Under certain conditions, the soliton of the fiber lasers can exhibit period-doubling bifurcation[38–40]. Although lots of work have revealed many characteristics of the
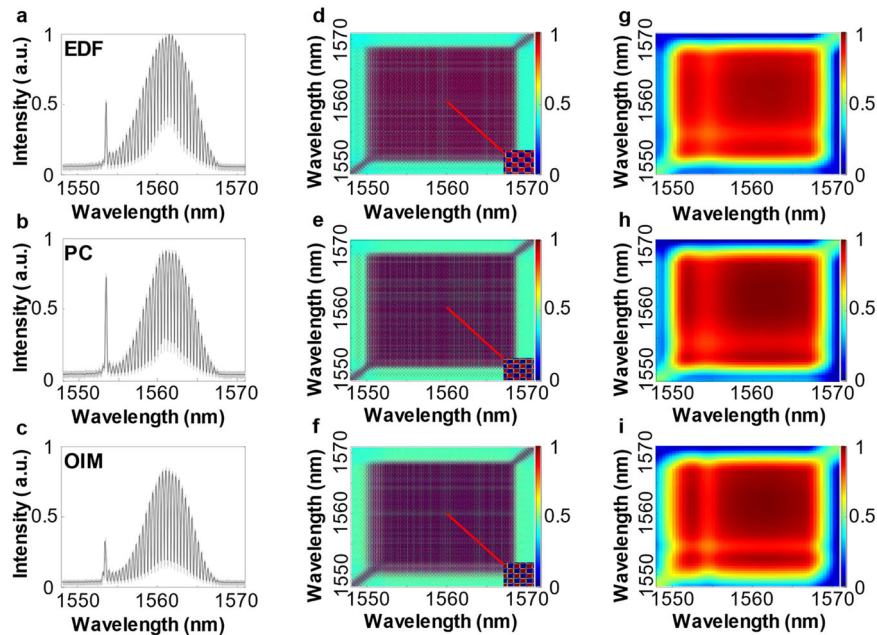
Fig. 5 Spectral coherence of solitons output from different ports. a–c The one-dimensional interference fringe results of the EDF port, PC port, and OIM port. The one-dimensional spectral coherence increases sequentially. EDF: erbium-doped fiber; PC: polarization controller; OIM: optical integrated module. **d–f** The two-dimensional interference fringe results. The zoom-in image around the central wavelength shows well-defined square-grid pattern with high contrast, indicating their coherence are quite well. **g–i** The estimated cross-spectral densities calculated from (**d–f**). The closer the color is to red, the closer the CSD is to 1, which means better spectral coherence. The two-dimensional spectral coherence also increases sequentially.

Table 2 The parameters used in the numerical simulation of the period-doubling bifurcation.

	SMF	EDF	HI1060	DCF
$\theta = 60/180\pi$	$\beta_2 = -21.7 \text{ ps}^2 \text{ km}^{-1}$	$\beta_2 = 40 \text{ ps}^2 \text{ km}^{-1}$	$\beta_2 = -11.4 \text{ ps}^2 \text{ km}^{-1}$	$\beta_2 = 160.37 \text{ ps}^2 \text{ km}^{-1}$
$\varphi = 21/360\pi$	$\beta_3 = 0.1302 \text{ ps}^3 \text{ km}^{-1}$	$\gamma = 0.0066 \text{ W}^{-1}$	$\beta_3 = 0.1302 \text{ ps}^3 \text{ km}^{-1}$	$\beta_3 = -0.98 \text{ ps}^3 \text{ km}^{-1}$
$L_b = 1 \text{ m}$	$\gamma = 0.00146 \text{ W}^{-1}$	Gaussian shape	$\gamma = 0.00165 \text{ W}^{-1}$	$\gamma = 0.002 \text{ W}^{-1}$
$\lambda_0 = 1560 \text{ nm}$	$L = 9.75 \text{ m}$	FWHM = 30 nm	$L = 0.5 \text{ m}$	$L = 0.5 \text{ m}$
		$g_0 = 20 \text{ m}^{-1}$		Loss = 3.4 dB
		$L = 0.6 \text{ m}$		
		$E_s = 120 \text{ pJ}$		

SMF single-mode fiber, *EDF* erbium-doped fiber. HI1060: Corning HI1060 fiber, *DCF* dispersion compensating fiber.

period-doubled solitons, there are still some possible complexities of soliton dynamics that have not been presented. A natural question is how period-doubled solitons can evolve from one state to another. For this reason, after a simple modification of the laser (see Table 2), the evolution process of period-doubled solitons in the cavity has been successfully demonstrated using the multi-port observation (Fig. 6a). The establishment process includes modulation instability, multi-solitons, spectral beating, and period-doubling bifurcation. After 4500 RT, the period-doubling bifurcation process becomes stable. The round-trip-resolved field autocorrelation function (ACF) calculated from the inverse Fourier transform of the single-shot spectra measured by the DFT technique[40,41] shows the output is a single soliton. The zoom-in image of 4900~4950 RT shown in the inset demonstrates the process of alternating the pulse width every other round trip, which indicates that the laser operates in a period-2 state. Compared with single-port observation in the inset of Fig. 6b, multi-port observation can not only observe the spectral expanding and shrinking alternately and periodically over roundtrips but also reflect the process of soliton evolution from period-1 to period-2 in the cavity. Especially, for the PC port, the concave spectra indicate that SPM makes an important contribution to the spectral evolution of period-2. The period-doubling bifurcation of multiple solitons is also observed by slightly increasing the pump power and carefully

adjusting the PC, as shown in Fig. 6c. The laser also operates in a period-2 state, and the spectra and evolution processes are similar to those of single solitons, except that the spectra show obvious comb-like modulation (Fig. 6d).

To further study this phenomenon, the simulation parameters are modified based on the modified laser parameters, and the period-2 state of a single soliton is successfully reproduced (Fig. 6e). In period-1 (381RT and 383RT), due to gain filtering, the expanded spectra gradually shrink as it is amplified. Subsequently, SPM and dispersion gradually reach equilibrium and soliton evolves stably. During this process, the spectra mainly show a difference in power. For period-2 (382 RT and 384 RT), the pulse is rapidly amplified in EDF, and the peak power is much higher than period-1. SPM enhancement results in spectral distortion, showing the expanded spectrum. Then, the loss of DCF reduces the overall pulse energy, and normal dispersion also broadens the pulse, leading to the weakening of SPM. During this process, the pulse appears in a distinct breathing state, but the spectra do not change much. Then the positive chirp induced by DCF is gradually compensated in SMF and temporal compression results in the SPM increasing. The spectra gradually become more concave until the pulse begins to broaden again. Finally, the spectra flatten out. The simulation results are qualitatively consistent with the experimental results,
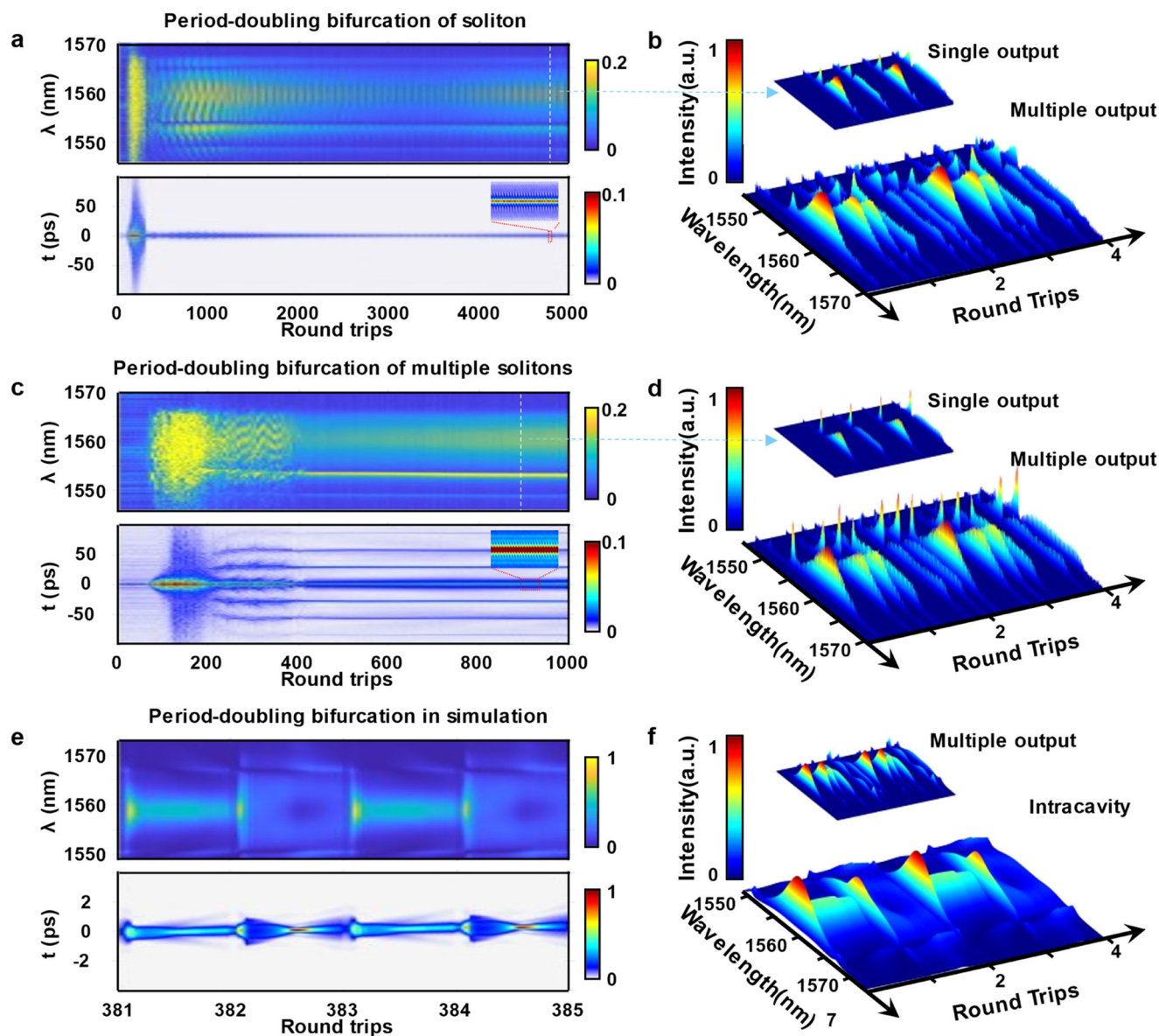
Fig. 6 The soliton dynamics of period-doubling bifurcation. a The real-time evolution process (above) and autocorrelation function (below) of a single soliton from OIM port. The zoom-in image in the inset indicates that the laser operates in a period-2 state. **b** The reconstituted spectra of the round trips by the white dashed line in **a** (RTs ~4900–4903). Compared with single-port observation, multi-port observation can reflect more details of soliton evolution from period-1 to period-2. **c** The real-time evolution process (above) and autocorrelation function (below) of multiple solitons from OIM port. **d** The reconstituted spectra of the round trips by the white dashed line in (**c**) (RTs ~901–904). The spectra and evolution processes are similar to those of single solitons, except that the spectra show obvious comb-like modulation. **e** The complete evolution of the spectra (above) and the time domain (below) in the cavity from simulation. **f** The 3D diagram shows a more clearly intracavitary evolution dynamics and the multi-port observation captures the important spectral features.

and the discrepancies such as the degree of concave in the spectra and the central wavelength, is mainly due to the fact that the simulation parameters cannot be exactly consistent with the experimental conditions. The 3D diagram in Fig. 6f shows a more clearly intracavitary evolution dynamics during period-doubling bifurcation. The multi-port observation shown in the inset captures the important spectral features and based on these distinct spectra, we can indeed have a more complete and realistic understanding of the intracavitary evolution processes.

Discussion
By introducing the multi-port observation into the DFT technique, the continuity and periodicity of the intracavitary evolution process in a mode-locked fiber laser are revealed. Compared with previous works, multi-port real-time observation can minify the interval of observation windows and relax the limitation of the insufficient sampling rate; therefore, intracavitary evolution dynamics that are not synchronized with soliton can be characterized. Owing to the accurate synchronicity of the stretched spectra, the periodic evolution of the sub-nanosecond pulse in the modulation instability stage, the sinusoidal evolution of the spectral beating process, the beating process of the Kelly sidebands, the beating and shifting process of the SPM peaks, and the intracavity dynamics of the period-doubling bifurcation are well demonstrated, which indicate that rich nonlinear dynamics can be embedded in the evolution of pulses in the cavity.

In conclusion, these ultrafast intracavitary phenomena indicate that the difference of soliton in different positions in the cavity are natural and ubiquitous in all stages of evolution. Under certain conditions, these differences can be evident, and these different intracavitary states are worthy of attention. The demonstrated multi-port real-time observation provides insights into exploring intracavity dynamics in various optical systems, which are helpful to understand the complex transient nonlinear dynamics in the cavity and complete the theories of soliton. On the other hand, it also has promise for studying how the solitons evolve between multiple states in other types of fiber lasers, such as Mamyshev oscillator[42], bidirectional all-normal dispersion fiber laser[43], and dissipative soliton resonance generation[44].

Methods

Pulse propagation within the fiber sections is modeled with the coupled Ginzburg-Landau equations (CGLE)[45,46]:

$$\frac{\partial u}{\partial z} = i\beta u - \delta\frac{\partial u}{\partial t} - \frac{i\beta_2}{2}\frac{\partial^2 u}{\partial t^2} + \frac{\beta_3}{6}\frac{\partial^3 u}{\partial t^3} + i\gamma(|u|^2 + \frac{2}{3}|v|^2)u + \frac{i\gamma v^2 u^*}{3} + \frac{gu}{2} + \frac{g}{2\Omega^2}\frac{\partial^2 u}{\partial t^2} \tag{1.1}$$

$$\frac{\partial v}{\partial z} = -i\beta v + \delta\frac{\partial v}{\partial t} - \frac{i\beta_2}{2}\frac{\partial^2 v}{\partial t^2} + \frac{\beta_3}{6}\frac{\partial^3 u}{\partial t^3} + i\gamma(|v|^2 + \frac{2}{3}|u|^2)v + \frac{i\gamma u^2 v^*}{3} + \frac{gv}{2} + \frac{g}{2\Omega^2}\frac{\partial^2 v}{\partial t^2} \tag{1.2}$$

Here, u and v are normalized slow-varying envelopes of the electric fields polarized along the two principal axes. $\beta = \pi/L_b$ is half the wavenumber difference between the fast-axis and slow-axis components, and L_b is the average linear birefringence beat length of the fiber laser resonator. $2\delta = \lambda_0/(cL_b)$ is the linear group-velocity difference between the two polarization modes. β_2 is the dispersion of the fiber and β_3 is the third-order dispersion. γ is the nonlinear coefficient of the fiber. The gain terms represent linear gain as well as a Gaussian approximation to the gain profile with the bandwidth Ω. The gain is described as

$g = g_0 \exp\left[-\frac{\int(|u|^2 + |v|^2)dt}{E_s}\right]$, which only exists in EDF. g_0 is the small-signal gain and E_s is the gain saturation energy related to pump power.

The effects of PC and OIM are described by transmission matrices $M_1 = \begin{bmatrix} \exp(i\varphi) & 0 \\ 0 & 1 \end{bmatrix}$ and $M_2 = \begin{bmatrix} \cos^2\theta & \sin(2\theta)/2 \\ \sin(2\theta)/2 & \sin^2\theta \end{bmatrix}$ respectively, where φ is the additional phase shift introduced by the PC, and θ is the angle between the polarization direction of the OIM and the slow axis of the fiber.

Data availability

The data that support the findings of this study are available from the corresponding author upon reasonable request.

References

1. Grelu, P. & Akhmediev, N. Dissipative solitons for mode-locked lasers. *Nat. Photon.* **6**, 84–92 (2012).
2. Krupa, K., Nithyanandan, K., Andral, U., Tchofo-Dinda, P. & Grelu, P. Real-time observation of internal motion within ultrafast dissipative optical soliton molecules. *Phys. Rev. Lett.* **118**, 243901 (2017).
3. Liu, X., Yao, X. & Cui, Y. Real-time observation of the buildup of soliton molecules. *Phys. Rev. Lett.* **121**, 023905 (2018).
4. Liao, R., Song, Y., Chai, L. & Hu, M. Pulse dynamics manipulation by the phase bias in a nonlinear fiber amplifying loop mirror. *Opt. Exp.* **27**, 14705–14715 (2019).
5. Du, Y. & Shu, X. Dynamics of soliton explosions in ultrafast fiber lasers at normal-dispersion. *Opt. Exp.* **26**, 5564–5575 (2018).
6. Soto-Crespo, J. M., Akhmediev, N. & Ankiewicz, A. Pulsating, creeping, and erupting solitons in dissipative systems. *Phys. Rev. Lett.* **85**, 2937–2940 (2000).
7. Mahjoubfar, A. et al. Time stretch and its applications. *Nat. Photon.* **11**, 341–351 (2017).
8. Ropers, C., Herink, G., Kurtz, F., Jalali, B. & Solli, D. Real-time spectral interferometry probes the internal dynamics of femtosecond soliton molecules. *Science* **356**, 50–54 (2017).
9. Chen, H. et al. Buildup dynamics of dissipative soliton in an ultrafast fiber laser with net-normal dispersion. *Opt. Exp.* **26**, 2972–2982 (2018).
10. Wei, X. et al. Unveiling multi-scale laser dynamics through time-stretch and time-lens spectroscopies. *Opt. Exp.* **25**, 29098 (2017).
11. Ryczkowski, P. et al. Real-time full-field characterization of transient dissipative soliton dynamics in a mode-locked laser. *Nat. Photon.* **12**, 221–227 (2018).
12. Runge, A. F. J., Broderick, N. G. R. & Erkintalo, M. Observation of soliton explosions in a passively mode-locked fiber laser. *Optica* **2**, 36–39 (2015).
13. Peng, J. & Zeng, H. Soliton collision induced explosions in a mode-locked fibre laser. *Commun. Phys.* **2**, 34 (2019).
14. Guo, Y. et al. Real-time multispeckle spectral-temporal measurement unveils the complexity of spatiotemporal solitons. *Nat. Commun.* **12**, 67 (2021).
15. Cao, Y. et al. Experimental revealing of asynchronous transient-soliton buildup dynamics. *Opt. Laser Technol.* **133**, 106512 (2021).
16. Wei, Z. et al. Pulsating soliton with chaotic behavior in a fiber laser. *Opt. Lett.* **43**, 5965–5968 (2018).
17. Wang, Z., Nithyanandan, K., Coillet, A., Tchofo-Dinda, P. & Grelu, P. Optical soliton molecular complexes in a passively mode-locked fibre laser. *Nat. Commun.* **10**, 830 (2019).
18. Chen, H. et al. Dynamical diversity of pulsating solitons in a fiber laser. *Opt. Expr.* **27**, 28507–28522 (2019).
19. Peng, J. & Zeng, H. Triple-state dissipative soliton laser via ultrafast self-parametric amplification. *Phys. Rev. A.* **11**, 044068 (2019).
20. Sulimany, K. et al. Bidirectional soliton rain dynamics induced by casimir-like interactions in a graphene mode-locked fiber laser. *Phys. Rev. Lett.* **121**, 133902 (2018).
21. Liang, H. et al. Real-time dynamics of soliton collision in a bound-state soliton fiber laser. *Nanophotonics* **9**, 1921–1929 (2020).
22. Meng, F. et al. Intracavity incoherent supercontinuum dynamics and rogue waves in a broadband dissipative soliton laser. *Nat. Commun.* **12**, 5567 (2021).
23. Bale, B. G., Boscolo, S., Kutz, J. N. & Turitsyn, S. K. Intracavity dynamics in high-power mode-locked fiber lasers. *Phys. Rev. A.* **81**, 033828 (2010).
24. Luo, J. et al. Mechanism of spectrum moving, narrowing, broadening, and wavelength switching of dissipative solitons in all-normal-dispersion Yb-fiber lasers. *IEEE Photon. J.* **6**, 1–8 (2014).
25. Wang, Y. et al. Experimental observation of transient mode-locking in the build-up stage of a soliton fiber laser. *Chin. Opt. Lett.* **19**, 071401 (2021).
26. Zhao, L. et al. Dynamics of gain-guided solitons in a dispersion-managed fiber laser with large normal cavity dispersion. *Opt. Commun.* **281**, 3324–3326 (2008).
27. Han, D. et al. Simultaneous picosecond and femtosecond solitons delivered from a nanotube-mode-locked all-fiber laser. *Opt. Lett.* **39**, 1565–1568 (2014).
28. Huang, C. et al. Developing high energy dissipative soliton fiber lasers at 2 micron. *Sci. Rep.* **5**, 13680 (2015).
29. Peng, J. et al. Real-time observation of dissipative soliton formation in nonlinear polarization rotation mode-locked fibre lasers. *Commun. Phys.* **1**, 20 (2018).
30. Kudelin, I., Sugavanam, S. & Chernysheva, M. Pulse-onset dynamics in a bidirectional mode-locked fibre laser via instabilities. *Commun. Phys.* **3**, 202 (2020).
31. Yu, Y. et al. Behavioral similarity of dissipative solitons in an ultrafast fiber laser. *Opt. Lett.* **44**, 4813–4816 (2019).
32. Li, H., Ouzounov, D. G. & Wise, F. W. Starting dynamics of dissipative-soliton fiber laser. *Opt. Lett.* **35**, 2403–2405 (2010).
33. Chen, H. et al. Soliton booting dynamics in an ultrafast anomalous dispersion fiber laser. *IEEE Photon. J.* **10**, 1–9 (2018).
34. Liu, X., Popa, D. & Akhmediev, N. Revealing the transition dynamics from Q switching to mode locking in a soliton laser. *Phys. Rev. Lett.* **123**, 093901 (2019).
35. Herink, G., Jalali, B., Ropers, C. & Solli, D. R. Resolving the build-up of femtosecond mode-locking with single-shot spectroscopy at 90 MHz frame rate. *Nat. Photon.* **10**, 321–326 (2016).
36. Li, B. et al. Real-time observation of round-trip resolved spectral dynamics in a stabilized fs fiber laser. *Opt. Exp.* **25**, 8751–8759 (2017).
37. Xu, Y., Wei, X., Ren, Z., Wong, K. K. & Tsia, K. K. Ultrafast measurements of optical spectral coherence by single-shot time-stretch interferometry. *Sci. Rep.* **6**, 27937 (2016).
38. Zhao, L., Tang, D., Cheng, T. & Lu, C. Period-doubling of multiple solitons in a passively mode-locked fiber laser. *Opt. Commun.* **273**, 554–559 (2007).
39. Yan, M., Hao, Q., Shen, X. & Zeng, H. Experimental study on polarization evolution locking in a stretched-pulse fiber laser. *Opt. Exp.* **26**, 16086–16092 (2018).
40. Du, W. et al. Real-time observation of pulsating period-doubled vector solitons in a passively mode-locked fiber laser. *Opt. Exp.* **29**, 14101–14111 (2021).
41. Ryczkowski, P. et al. Real-time full-field characterization of transient dissipative soliton dynamics in a mode-locked laser. *Nat. Photon.* **12**, 221 (2018).

42. Yan, D., Li, X., Zhang, S. & Liu, J. Pulse dynamic patterns in a self-starting Mamyshev oscillator. *Opt. Exp.* **29**, 9805–9815 (2021).
43. Li, B. et al. Bidirectional mode-locked all-normal dispersion fiber laser. *Optica* **7**, 396304 (2020).
44. Du, W. et al. Polarization dynamics of dissipative-soliton-resonance pulses in passively mode-locked fiber lasers. *Opt. Exp.* **27**, 8059–8068 (2019).
45. Tang, D., Zhao, L., Zhao, B. & Liu, A. Q. Mechanism of multisoliton formation and soliton energy quantization in passively mode-locked fiber lasers. *Phys. Rev. A.* **72**, 043816 (2005).
46. Wu, J., Tang, D., Zhao, L. & Chan, C. C. Soliton polarization dynamics in fiber lasers passively mode-locked by the nonlinear polarization rotation technique. *Phys. Rev. E.* **74**, 046605 (2006).

Author contributions

The experiment was designed and implemented by Y.D., L.C., and Z.L. The multi-port fiber laser was co-developed by Y.D. and Z.L., and the numerical simulation was co-developed by Y.D. and L.Z. C.Z., L.Z., and X.Z. developed the concept and supervised measurements and analysis. All authors contribute the preparation of the manuscript.

Competing interests

The authors declare no competing interests.

Additional information

Correspondence and requests for materials should be addressed to Chi Zhang, Luming Zhao or Xinliang Zhang.

Peer review information *Communications Physics* thanks the anonymous reviewers for their contribution to the peer review of this work.

Reprints and permission information is available at http://www.nature.com/reprints

Publisher's note Springer Nature remains neutral with regard to jurisdictional claims in published maps and institutional affiliations.